Reaffirming the d_{x^{2}-y^{2}} Superconducting Gap Using the Autocorrelation Angle-Resolved Photoemission Spectroscopy of Bi_{1.5}Pb_{0.55}Sr_{1.6}La_{0.4}CuO_{6+δ}

M. Hashimoto, R.-H. He, J. P. Testaud, W. Meevasana, R. G. Moore, D. H. Lu, Y. Yoshida, H. Eisaki, T. P. Devereaux, Z. Hussain, and Z.-X. Shen

Phys. Rev. Lett. **106**, 167003 — Published 22 April 2011

DOI: 10.1103/PhysRevLett.106.167003

Reaffirming the $d_{x^2-y^2}$ superconducting gap using the auto-correlation angle-resolved photoemission spectroscopy of $Bi_{1.5}Pb_{0.55}Sr_{1.6}La_{0.4}CuO_{6+\delta}$

M. Hashimoto,[1,2,3,4] R.-H. He,[2,3,4] J. P. Testaud,[2,3,4] W. Meevasana,[2,3] R. G. Moore,[1,2,3] D. H. Lu,[1] Y. Yoshida,[5] H. Eisaki,[5] T. P. Devereaux,[2,3] Z. Hussain,[4] and Z.-X. Shen[2,3]

[1] *Stanford Synchrotron Radiation Lightsource, SLAC National Accelerator Laboratory, 2575, Sand Hill Road, Menlo Park, California 94025, USA*

[2] *Stanford Institute for Materials and Energy Sciences, SLAC National Accelerator Laboratory, 2575 Sand Hill Road, Menlo Park, CA 94025, USA*

[3] *Geballe Laboratory for Advanced Materials, Departments of Physics and Applied Physics, Stanford University, CA 94305, USA*

[4] *Advanced Light Source, Lawrence Berkeley National Lab, Berkeley, CA 94720, USA*

[5] *Nanoelectronics Research Institute, AIST, Ibaraki 305-8568, Japan*

(Dated: April 4, 2011)

Knowledge of the gap function is important to understand the pairing mechanism for high-temperature (T_c) superconductivity. However, Fourier transform scanning tunneling spectroscopy (FT-STS) and angle-resolved photoemission spectroscopy (ARPES) in the cuprates have reported contradicting gap functions, with FT-STS results deviating strongly from a canonical $d_{x^2-y^2}$ form. We study this problem by applying an "octet model" analysis to auto-correlation (AC) ARPES. The results suggest that a contradiction occurs because the octet model does not consider the effects of matrix elements and the pseudogap. This re-affirms the canonical $d_{x^2-y^2}$ functional form for the superconducting gap around the node below T_c, which can be directly determined from ARPES. Further, our study suggests that the FT-STS reported persistence of the fluctuating superconductivity around the node at far above T_c is not necessary to explain the existence of the quasi-particle interference at low energy.

PACS numbers: 74.72.-h, 74.25.Jb, 74.55.+v

The superconducting gap magnitude in a superconductor reflects the pairing strength of a Cooper pair, which is closely related to the transition temperature (T_c). Because of that, the experimental determination of the gap magnitude is vitally important to understand the mechanism of superconductivity. In high-T_c cuprate superconductor, the momentum ($\mathbf{k}$) dependence of the gap has to be determined at the same time. However, two complementary leading tools for such information, angle-resolved photoemission spectroscopy (ARPES) and Fourier transform scanning tunneling spectroscopy (FT-STS), have reported inconsistent gap functions. While all ARPES studies have consistently indicated the presence of nodal $d_{x^2-y^2}$ excitations below T_c [1–6], FT-STS studies have reported finite gapless "Fermi arcs" [7–11], which persists well above T_c with no signature across the superconducting transition [12]. These momentum and temperature dependences of an FT-STS derived gap function also conflict with transport, and suggests a more complex nature for high-T_c superconductivity. Given the high influence of these experimental tools and the issue whether the superconducting fluctuation extends well above T_c, it is important to ascertain the gap functional form for a successful development of a microscopic theory.

STS is a real-space ($\mathbf{r}$-space) probe that can visualize $\mathbf{k}$-space properties via FT-STS. When quasi-particles scatter off impurities, a quasi-particle standing wave interference (QPI) pattern is formed in $\mathbf{r}$-space, that modulates the density of states and is most clearly displayed in momentum transfer ($\mathbf{q}$) space via the FT of the $\mathbf{r}$-space image. In the octet model for d-wave superconductors [13–16], eight $\mathbf{k}$-space points at the same energy on the Fermi surface (FS) within the first Brillouin zone are connected by seven vectors in momentum transfer ($\mathbf{q}$) space $\mathbf{q}_1$ to $\mathbf{q}_7$, which are associated with the superconducting gap size at the respective $\mathbf{k}$-space points [7–12]. We emphasize that FT-STS is reliant on the octet model to obtain the gap function, in contrast to the direct determination of the gap by ARPES.

It has been reported STS matrix elements suppress the nodal region in $\mathbf{k}$-space [17–20]. This could explain why the FT-STS gap function obtained from octet-model analysis lacks information around the node [7–12]. However, such matrix element effects have not been studied extensively because they are difficult to determine experimentally. A possible way to approach this issue is to investigate the auto-correlation (AC) of ARPES intensities in $\mathbf{q}$-space $I_{AC}(\mathbf{q},\omega) = \int I(\mathbf{k},\omega)I(\mathbf{k}+\mathbf{q},\omega)d\mathbf{k}$, which has been interpreted as joint density of states (JDOS) $\int A(\mathbf{k},\omega)A(\mathbf{k}+\mathbf{q},\omega)d\mathbf{k}$. Here, ARPES intensity is $I(\mathbf{k},\omega) = M(\mathbf{k},h\nu,\mathbf{A})A(\mathbf{k},\omega)f(\omega,T)$ where $M(\mathbf{k},h\nu,\mathbf{A})$ are matrix elements, $A(\mathbf{k},\omega)$ is spectral function, and $f(\omega,T)$ is Fermi-Dirac function. While not the same, the theoretical similarity between JDOS and QPI has been pointed out [13–16] and the experimental comparisons between FT-STS and AC-ARPES have supported it [21, 22].

In this letter, to obtain AC-ARPES intensities, we use an ARPES data set of nearly optimally-doped $Bi_{1.5}Pb_{0.55}Sr_{1.6}La_{0.4}CuO_{6+\delta}$ (Pb-Bi2201, $T_c = 38$ K, the

pseudogap temperature T^* ∼ 140 K) [23]. Here we stress that we choose an experimental condition where the nodal spectral intensities are suppressed by matrix elements [23], utilizing the fact that matrix elements highly depend on incident photon energy and polarization [24]. This is similar to the STS theoretical expectation [17–20] and thus allows us to discuss the STS observations, especially the FT-STS derived gap function. We show that, the obtained AC-ARPES intensities are severely affected by the convoluted effect of intrinsic spectral widths, the pseudogap and matrix elements. Eventually, applying the octet model, which does not take such effects into consideration, induces a form of the gap function that differs from ARPES, but is very similar to the FT-STS [7–11] and temperature-dependent FT-STS [12] results. Our result re-affirms the $d_{x^2-y^2}$ superconducting gap function near the node below T_c, which is consistent with previous ARPES studies [1–6].

The **k**-space ARPES intensities of Pb-Bi2201 at E_F at different temperatures are shown in Fig. 1(a)-(c). At 172 K ($> T^*$), where no gap exists, the intensity near the node ∼$(\pi/2, \pi/2)$ is very weak compared to the antinodal region ∼$(\pi, 0)$ intensity. This confirms that the present experimental condition suppresses the nodal region intensity similar to the STS theoretical expectation [17–20]. From these **k**-space ARPES intensities with strong matrix element effects, we obtain the **q**-space AC-ARPES intensities at different energies as shown in Fig. 1(d)-(o). At 8 K ($\ll T_c$), there exist high-intensity spots which can be attributed to the octet-model **q**-vectors $\mathbf{q}_1$–$\mathbf{q}_7$ at low binding energies ($\lesssim -20$ meV). Here we define $\mathbf{q}_1$–$\mathbf{q}_7$ as indicated in Fig. 1(d) and these vectors can be associated with the vectors between the high-intensity spots in **k**-space as exemplified in Fig. 1(a). At higher binding energy, the existence of $\mathbf{q}_1$–$\mathbf{q}_7$ becomes less clear and, instead, the broader spots defined as $\mathbf{q}_3^*$ and $\mathbf{q}_5^*$ appear[Fig. 1(m)]. Upon raising the temperature above T_c, one can still see $\mathbf{q}_1$–$\mathbf{q}_7$ as shown in Fig. 1(e), but they completely disappear above T^*. On the other hand, $\mathbf{q}_3^*$ and $\mathbf{q}_5^*$ show little temperature dependence. At $T > T^*$ where neither the superconductivity nor pseudogap exists, one can only find $\mathbf{q}_3^*$ and $\mathbf{q}_5^*$ at all the energies [Fig. 1(f), (i), (l) and (o)].

Next, we extract the energy dispersion of the **q**-vectors [23]. In the AC-ARPES high symmetry cuts below T_c shown in Fig. 2(a) and (b), $\mathbf{q}_1$–$\mathbf{q}_7$ show clear dispersion ($\gtrsim -18$ meV) as expected in the octet model. At higher binding energy (< -30 meV), $\mathbf{q}_3^*$ and $\mathbf{q}_5^*$ replace $\mathbf{q}_1$–$\mathbf{q}_7$. $\mathbf{q}_1$–$\mathbf{q}_7$ show dispersion also at 45 K ($> T_c$) with small change of $|\mathbf{q}|$ from those at 10 K, but become harder to track at higher binding energy (< -8 meV) as shown in Fig. 2(c) and (d). Notably, Fig. 2(e) and (f) reveal that, even above T^*, $\mathbf{q}_3^*$ and $\mathbf{q}_5^*$ dominate for all energies. These **q**-vectors show weak but finite dispersions reflecting the bare band structure. Although the overall features look similar, this is different from the FT-STS

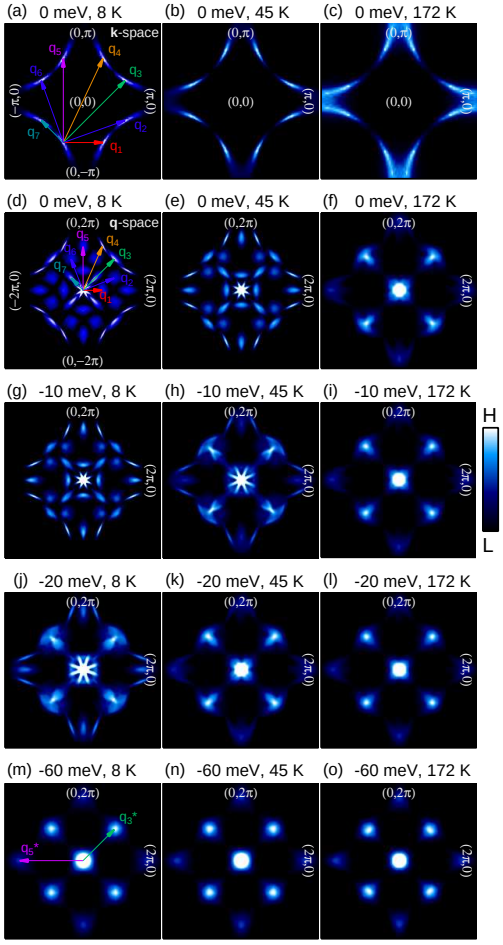

FIG. 1. (Color online) Image plots in **k**- and **q**-spaces of nearly optimally-doped Pb-Bi2201. (a)-(c) **k**-space ARPES intensities at 0 meV (E_F) for three temperatures, 8 K ($< T_c$), 45 K ($T_c < T \ll T^*$) and 172 K ($> T^*$), respectively. (d)-(o), **q**-space AC-ARPES intensities at various energies for the three temperatures as denoted. All the intensities are integrated within ±0.5 meV. $\mathbf{q}_1 - \mathbf{q}_7$ in **q**-space are exemplified in (d) in appropriate colors, which are the **q**-vectors expected for the octet model. Corresponding **q**-vectors in **k**-space are indicated in (a). Definitions of $\mathbf{q}_3^*$ and $\mathbf{q}_5^*$ at higher binding energy in **q**-space are shown in (m).

observation of the energy independent **q** vectors at higher energy below T^*. They have been associated with the density-wave-like pseudogap [25, 26].

Applying the octet model analysis to the extracted $\mathbf{q}_1$–$\mathbf{q}_7$ at 10 K and 45 K, as summarized in Fig. 2(g) and (h), the gap function and the minimum gap loci (MGLs) which reflect the FS shape can be reconstructed and compared to the results obtained from a direct ARPES analysis [23]. As shown in Fig. 3(a), the two methods show a consistent FS shape for all temperatures although the MGLs from AC-ARPES are limited to a more narrow region of **k**-space. This suggests that $\mathbf{q}_1$–$\mathbf{q}_7$ track the

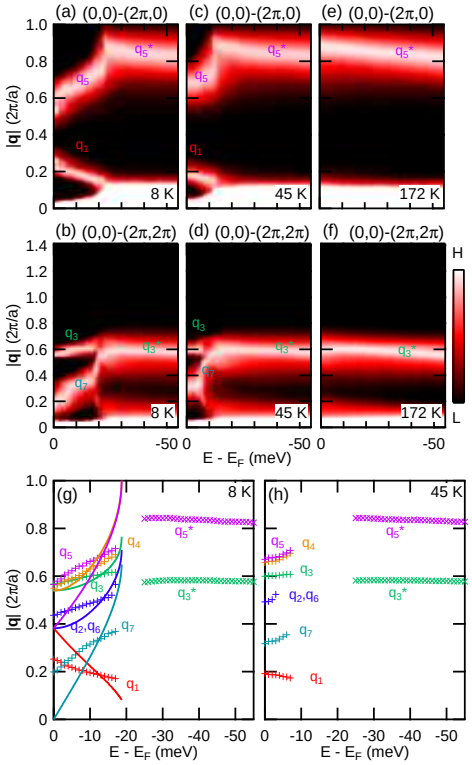

FIG. 2. (Color online) Energy dispersions of the **q**-vectors from AC-ARPES. (a)-(f) Energy dependences of AC-ARPES intensities along high-symmetry **q** directions at 8 K ($< T_c$), 45 K ($T_c < T \ll T^*$), and 172 K ($> T^*$), as denoted. The intensities at each energy are normalized to the height of $\mathbf{q}_5$ (or $\mathbf{q}_5^*$) in (a), (c) and (e), and $\mathbf{q}_3$ (or $\mathbf{q}_3^*$) in (b), (d) and (f), respectively, for visualization purposes. (g) and (h) Summary of the extracted dispersions of the **q**-vectors at 8 K ($< T_c$) and 45 K ($T_c < T \ll T^*$), respectively. Solid curves in g are the dispersions of $\mathbf{q}_1$–$\mathbf{q}_7$ for a $d_{x^2-y^2}$ gap $\Delta_{sc}(\mathbf{k}) = \Delta_{max}|\cos(k_x) - \cos(k_y)|/2$ ($\Delta_{max} = 19$ meV). The same colors as Fig. 1 are used for the symbols and labels of the **q**-vectors.

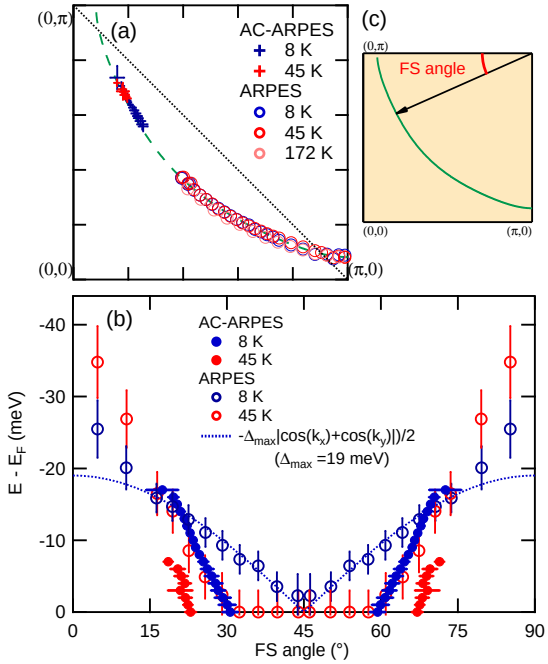

FIG. 3. (Color online) Deviation from the $d_{x^2-y^2}$ gap anisotropy in the octet model analysis of AC-ARPES. (a) Comparison of the FS shape obtained from the two different analysis methods applied to the same data at various temperatures. Dashed curve and dotted line are eye-guide for the FS shape and the anti-ferromagnetic Brillouin zone boundary, respectively. (b) Comparison of the gap anisotropy between the two methods. The definition of the FS angle is shown in (c). Dotted curve in (b) is for the $d_{x^2-y^2}$ gap function ($\Delta_{max} = 19$ meV). The energy ranges for the FS shape from AC-ARPES in (a) are the same as those for the gap functions in (b).

electronic properties approximately along the FS and the observation of $\mathbf{q}_1$–$\mathbf{q}_7$ is because of the existence of a gap about E_F as they are not observed above T^* [Fig. 2(e) and (f)]. However, the gap anisotropies from the two methods show apparently different behaviors as seen in Fig. 3(b). At $T < T_c$, the ARPES derived gap anisotropies show a simple canonical $d_{x^2-y^2}$ form with point nodes at the zone diagonal consistent with the previous ARPES studies [1–6], while the octet model analysis suggests the absence of the gap near the node (formation of a Fermi arc). In addition, the gap function near the antinode is lost. The AC-ARPES derived gap anisotropy does not abruptly change when crossing T_c from below. The ungapped Fermi arc region becomes larger but the overall feature is maintained. This is well contrasted with the abrupt gap closing and the formation of the Fermi arc above T_c in the ARPES derived gap function. While the two methods show inconsistent gap functions, the AC-ARPES derived gap function is very similar to the one from FT-STS [7–12] both in terms of a momentum and temperature dependences [12].

We first discuss the most critical difference of the gap function around the node between the two methods. In the octet model, the canonical $d_{x^2-y^2}$ gap function expects the merger of $\mathbf{q}_1$–$\mathbf{q}_7$ into 3 vectors at E_F as indicated by the solid curves in Fig. 2(g), as the gap is closed only at the node. This means that there exist at E_F only 4 high-intensity spots at the nodes in the **k**-space image plot. However, even though we observed a gap closing only at the node from ARPES [23], simultaneously, we clearly observed 8 high-intensity spots away from the node at E_F as shown in Fig. 1(a). They generate the 7 **q**-vectors in the AC-ARPES intensities [Fig. 1(d)], and consequently, the MGL and gap function terminate before reaching the node, giving an apparent Fermi arc like feature even below T_c.

These seemingly contradictory observations in the

same data (the gap closure at the node and the 8 high-intensity spots at E_F in **k**-space) can be understood by considering the compounded effect of intrinsic spectral widths and matrix elements. Because of the spectral widths by lifetime broadening due to intrinsic and extrinsic scattering, outside the node, ARPES can have finite intensities at E_F. If the **k**-dependence of the matrix elements is strong enough as in the present experimental condition or STS theoretical expectation [17–20], these intensities away from the node can be stronger than those at the nodes, and eventually give 8 high-intensity spots even at E_F.

To conclude, as we demonstrated, the **q**-space spectra both from AC-ARPES and FT-STS give an incorrect gap function, because the octet model relies on the **q**-space intensity variation and ignores the effects of intrinsic spectral widths and matrix elements. The similar but inaccurate gap function from AC-ARPES and FT-STS may be understood as a result of similar matrix elements. By manipulating matrix elements, it is further confirmed that the octet model gap function is strongly influenced by matrix elements [23]. On the other hand, the gap function directly determined from ARPES does not suffer from matrix elements because each ARPES spectrum at a fixed momentum is evaluated individually and the relative intensities between different momenta does not affect the gap determination.

Our results suggest that the gap function in the antinodal region is affected by the existence of the pseudogap in addition to the effects discussed above. Interestingly, $\mathbf{q}_1$–$\mathbf{q}_7$ are clearly observed even slightly above T_c, similar to the recent FT-STS report [12]. This suggests that $\mathbf{q}_1$–$\mathbf{q}_7$ are affected by the pseudogap physics, indicating that the observation of $\mathbf{q}_1$–$\mathbf{q}_7$ is not sufficient to conclude whether the pseudogap is fluctuating superconductivity or competing order. Further, as shown in Fig. 3(b), the AC-ARPES gap function changes continuously across T_c, suggesting that the gap function from AC-ARPES in the superconducting state [Fig. 3(b)] is also affected by the existence of the pseudogap, but the effect of the superconducting gap that opens on the Fermi arc is not strong. We may conclude that the existence of the QPI above T_c does not necessarily require fluctuating superconductivity near the node, but could be consistent with fluctuating superconductivity in the antinodal region [27]. Moreover, the destruction of the octet model features near the antinode is consistent with the suppression of the spectral weight [3, 28] and/or band renormalization in the antinodal region by the pseudogap [28]. The termination point may not be directly related to the antiferromagnetic zone boundary, as reported via STS [11].

In summary, we showed that, unlike the ARPES extracted result, the gap function from AC-ARPES as well as FT-STS are inaccurate due to the compounded effect of intrinsic spectral widths, the pseudogap and matrix elements. Further, our results suggest the more general importance of such effects when investigating **k**-space electronic structure from **r**- and **q**-space information. This may reconcile ARPES and FT-STS results and suggests that the superconductivity is triggered by the superconducting gap opening on the Fermi arc with a simple $d_{x^2-y^2}$ functional form. This contradicts the STS proposal of superconductivity with the Fermi arc and with no sharp signature of a superconducting transition. It is likely that the observance of QPI above T_c may mainly be caused by a gap in the antinodal region, and the lack of sensitivity to states near the nodal region.

We thank W.-S. Lee, A. Fujimori, P. Hirschfeld D. Scalapino, E. Abrahams and S. Kivelson for helpful discussions and Y. Li for experimental assistance on SQUID measurements. R.-H.H. thanks the SGF for financial support. This work is supported by the Department of Energy, Office of Basic Energy Science under contract DE-AC02-76SF00515.

[1] K. Tanaka *et al.*, Science **314**, 1910 (2006).
[2] W. S. Lee *et al.*, Nature **450**, 81 (2007).
[3] T. Kondo *et al.*, Nature **457**, 296 (2009).
[4] A. Kanigel *et al.*, Phys. Rev. Lett. **99**, 157001 (2007).
[5] U. Chatterjee *et al.*, Nature Phys. **6**, 99 (2010).
[6] A. Damascelli, Z. Hussain, and Z.-X. Shen, Rev. Mod. Phys. **75**, 473 (2003).
[7] J. E. Hoffman *et al.*, Science **297**, 1148 (2002).
[8] K. McElroy *et al.*, Nature **422**, 592 (2003).
[9] T. Hanaguri *et al.*, Nature Phys. **3**, 865 (2007).
[10] W. D. Wise *et al.*, Nature Phys. **5**, 213 (2009).
[11] Y. Kohsaka *et al.*, Nature **454**, 1072 (2008).
[12] J. Lee *et al.*, Science **325**, 1099 (2009).
[13] Q. H. Wang and D. H. Lee, Phys. Rev. B **67**, 020511 (2003).
[14] R. S. Markiewicz, Phys. Rev. B **69**, 214517 (2004).
[15] D. Wulin, Y. He, C.-C. Chien, D. K. Morr and K. Levin, Phys. Rev. B **80**, 134504 (2009).
[16] D. Wulin, C.-C. Chien, D. K. Morr, and K. Levin, Phys. Rev. B (R) **81**, 100504 (2010).
[17] O. K. Andersen, A. Liechtenstein, O. Jepsen, and F. Paulsen, J. Phys. Chem. Solids **56**, 1573 (1995).
[18] C. Wu, T. Xiang, and Z.-B. Su, Phys. Rev. B **62**, 14427 (2000).
[19] I. Martin, A. V. Balatsky, and J. Zaanen, Phys. Rev. Lett. **88**, 097003 (2002).
[20] J. Nieminen, H. Lin, R. S. Markiewicz, and A. Bansil, Phys. Rev. Lett. **102**, 037001 (2009).
[21] K. McElroy *et al.*, Phys. Rev. Lett. **96**, 067005 (2006).
[22] U. Chatterjee *et al.*, Phys. Rev. Lett. **96**, 107006 (2006).
[23] See EPAPS Document No. [xxx] for supplemental information.
[24] A. Bansil, and M. Lindroos, Phys. Rev. Lett. **83**, 5154 (1999).
[25] J. E. Hoffman *et al.*, Science **295**, 466 (2002).
[26] W. D. Wise *et al.*, Nature Phys. **4**, 696 (2008).
[27] T. Kondo *et al.*, Nature Phys. **7**, 21 (2011).
[28] M. Hashimoto *et al.*, Nature Phys. **6**, 414 (2010).